Acta Crystallographica Section D
Biological Crystallography
ISSN 0907-4449

tRNA^{Ser} acceptor stem: conformation and hydration of a microhelix in a crystal structure at 1.8 Å resolution

Charlotte Förster,[a]‡ Arnd B. E. Brauer,[a]‡ Svenja Brode,[a]§ Jens P. Fürste,[a] Christian Betzel[b] and Volker A. Erdmann[a]*

[a]Institute of Chemistry and Biochemistry, Free University Berlin, Thielallee 63, 14195 Berlin, Germany, and [b]Institute of Biochemistry and Food Chemistry, University of Hamburg, c/o DESY, Notkestrasse 85, Building 22a, 22603 Hamburg, Germany

‡ These authors contributed equally.
§ Current address: Proteros Biostructures GmbH, Am Klopferspitz 19, 82152 Martinsried, Germany.

Correspondence e-mail: erdmann@chemie.fu-berlin.de

Received 27 July 2007
Accepted 14 September 2007

PDB Reference: tRNA^{Ser} acceptor stem, 2v6w, r2v6wsf.

The crystal structure of a serine-specific tRNA acceptor-stem microhelix, the binding site for the seryl-tRNA synthetase, was solved by X-ray analysis. This seven-base-pair tRNA^{Ser} microhelix forms endless rows of helices in the crystal lattice, with two helices stacking 'head-to-head' onto each other, resulting in an intermolecular guanosine stacking of the first purine nucleotides at the 5′-strands of the tRNA^{Ser} microhelices. A network of 75 water loci could be associated with each RNA duplex. Unusual local geometric backbone parameters could be detected in the region of the G4 phosphate located in the 5′-strand of the helix, which lead to a 'kink' in this region and to an irregularly bent helix. The role of the specific hydration pattern and of the irregular conformation of the tRNA^{Ser} acceptor-stem helix is discussed and summarized.

1. Introduction

Serine-specific elongator tRNAs participate in the elongation cycle of ribosomal protein biosynthesis and introduce the amino acid serine into the growing polypeptide chain. Owing to redundancy in the genetic code, six mRNA codons exist for serine and therefore different serine-specific tRNA isoacceptors also exist; five are currently listed in the tRNA-sequence database (Sprinzl & Vassilenko, 2005). All serine tRNAs are aminoacylated with serine by the same seryl-tRNA synthetase (Sunharadas *et al.*, 1968). This implies that all tRNA^{Ser} isoacceptors possess the same unique identity elements that determine the correct aminoacylation process. In addition, there is another tRNA that depends on seryl-tRNA synthetase aminoacylation: the UGA-suppressor tRNA^{Sec}, which is responsible for the co-translational insertion of selenocysteine into certain proteins (Leinfelder *et al.*, 1988; Böck *et al.*, 1991), is aminoacylated with serine by seryl-tRNA synthetase prior to conversion to selenocysteinyl-tRNA^{Sec} in a second enzymatic process (Forchhammer *et al.*, 1991; Forchhammer & Böck, 1991). The selenocysteine-specific tRNA^{Sec} also possesses identity elements determining serine aminoacylation as the first reaction prior to Sec-tRNA^{Sec} conversion. This communication addresses the question of the structural determinants that balance tRNA^{Ser} and tRNA^{Sec} amino-acid specificity.

The tRNA identity elements of seryl-tRNA synthetase are well known and have been investigated by a variety of genetic, biochemical and structural methods. The determinants consist of several distinct conserved regions in tRNA^{Ser}. As seryl-tRNA synthetase is a class II synthetase, it requires rather unique and simple determinants, excluding the anticodon, in

contrast to class I tRNA synthetases (Eriani *et al.*, 1990; Giegé *et al.*, 1998). The minimal consensus-sequence elements to assure serine identity include nucleotides at the top of the aminoacyl domain such as A3–U70, G2–C71, C72 and the discriminator base G73 and additionally C11–G24 in the D-stem (Normanly *et al.*, 1986, 1992; Normanly & Abelson, 1989; Schimmel, 1987). Interactions between seryl-tRNA synthetase and the 3′-end of $tRNA^{Ser}$ at positions C67, U68, C69 and U70 in the acceptor stem have also been determined by footprinting analysis (Schatz *et al.*, 1991), with additional contacts in the T-region. Small $tRNA^{Ser}$ microhelices derived from the acceptor stem can be recognized and aminoacylated by seryl-tRNA synthetase (Sampson & Saks, 1993). In addition, the presence of the long extra arm in $tRNA^{Ser}$ and $tRNA^{Sec}$ is important for specificity and is a main identity element that interacts with seryl-tRNA synthetase, with RNA backbone contacts to a conserved domain in the protein that are predominantly determined by the structure and length of the large extra arm (Normanly & Abelson, 1989; Normanly *et al.*, 1992). The role of the long extra arm as a main determinant for $tRNA^{Ser}$–synthetase interaction has also been demonstrated for an archaebacterial seryl-tRNA synthetase (Korencic *et al.*, 2004; Bilokapic *et al.*, 2006).

The crystal structure of $tRNA^{Ser}$ in complex with *Thermus thermophilus* seryl-tRNA synthetase has been analyzed at 2.9 Å and presents valuable information concerning the interaction of a class II tRNA synthetase with tRNA (Biou *et al.*, 1994; Cusack *et al.*, 1996). The protein interacts with the inside of the L-shaped three-dimensional structure of $tRNA^{Ser}$, with contacts being made to the long extra arm of the tRNA as well as to the aminoacyl stem, which carries the specific sequence identity elements. Intermolecular contacts are mainly described by tRNA-backbone interactions with the synthetase, including the long unique variable arm of the serine-specific tRNAs. However, some regions of $tRNA^{Ser}$ are not visible in the structure of the complex (PDB code 1ser; Biou *et al.*, 1994). These include the 5′- and 3′-ends of the aminoacyl stem, which carries the main identity elements for serine specificity, and also the GCCA-end. For a second structure (Cusack *et al.*, 1996) the resolution of the tRNA end could be improved to 2.7 Å. The main contacts of the $tRNA^{Ser}$ aminoacyl stem with the synthetase are between nucleotides G2–C71, C69, U68 and the amino acids from the loop 2 region of seryl-tRNA synthetase. The authors point out that there are rather few base-specific interactions between the tRNA acceptor stem and the synthetase and that the enzyme does not strongly discriminate the sequence of the tRNA acceptor stem. This is also consistent with the results of the footprinting analysis (Schatz *et al.*, 1991). Cusack and coworkers report a remarkable conformational change in the loop 2 region of the synthetase with respect to either tRNA binding or binding of the seryl-AMP substrate analogue 5′-*O*-[*N*-(L-seryl)-sulfamoyl]adenosine (Ser-AMS). These two conformations of the synthetase are described as the T- or A-conformation (Cusack *et al.*, 1996). The exact conformation of the 3′-CCA end, which accepts the amino acid, cannot be interpreted in this case owing to incomplete electron density in this structure. The authors noted that the acceptor stem, which consists of an 5′ all-purine strand and an 3′ all-pyrimidine strand, could possibly induce a particular helical conformation that is required by the synthetase. Thus, there is a need for a high-resolution structure of the $tRNA^{Ser}$ microhelix in order to analyze the specific local helical parameters in detail.

Further insights into tRNA–seryl-tRNA interaction were derived from docking $tRNA^{Tyr}$ into the crystal structure of archeabacterial *Methanosarcina barkeri* seryl-tRNA synthetase (Bilokapic *et al.*, 2006). In agreement with other biochemical and structural investigations, the long extra arm of the tRNA interacts with the two helices H1 and H2 within the N-terminal domain of the protein. Calculations including the electrostatic charge distribution suggest that the interactions of the synthetase with the tRNA mainly consist of contacts to the RNA phosphate backbone.

In order to investigate the high-resolution structure of the $tRNA^{Ser}$ aminoacyl domain, we crystallized and analyzed a $tRNA^{Ser}$ acceptor-stem microhelix 7-mer containing identity elements for serine specificity at 1.8 Å resolution. The role of hydration and specific water molecules in the tRNA microhelix, as well as some unusual RNA phosphate-backbone geometries, are discussed with respect to seryl-tRNA synthetase interaction.

2. Materials and methods

2.1. Crystallization and X-ray diffraction data

The synthesis, purification and crystallization of the $tRNA^{Ser}$ microhelix have been described previously (Förster *et al.*, 2006). Following hybridization of the two complementary RNA strands 5′-GGAGAGA-3′ and 5′-UCUCUCC-3′ to generate the $tRNA^{Ser}$ microhelix, crystallization occurred at a concentration of 0.5 m*M* RNA in 50 m*M* sodium cacodylate pH 6.0, 15 m*M* magnesium sulfate and 1.8 *M* lithium sulfate at 293 K in 24-well Linbro Plates (ICN Biomedicals Inc., Ohio, USA) using the hanging-drop vapour-diffusion technique. Crystals with approximate dimensions of $0.4 \times 0.1 \times 0.05$ mm appeared after three weeks. Prior to X-ray diffraction data collection, crystals were flash-frozen with liquid nitrogen in a cryoprotectant solution containing 50 m*M* sodium cacodylate pH 6.0, 15 m*M* magnesium sulfate, 1.8 *M* lithium sulfate and 20%(*v*/*v*) glycerol. X-ray diffraction data were collected on X-ray diffraction beamline XRD1 (5.2R) at the ELETTRA synchrotron, Trieste. Data processing and determination of the space group and unit-cell parameters were performed using the *HKL*-2000 package (Otwinowski & Minor, 1997).

2.2. Structure solution, refinement and analysis

The structure of the $tRNA^{Ser}$ acceptor-stem microhelix was solved by molecular replacement using the program *AMoRe* (Navaza, 1994) from the *CCP*4 package (Collaborative Computational Project, Number 4, 1994). We had no success with molecular replacement using the coordinates of small RNA crystal structures. Considering the general three-dimensional tRNA structure (Kim *et al.*, 1974; Quigley & Rich,

Table 1
Diffraction data and refinement statistics for the tRNA^{Ser} microhelix.

Values in parentheses are for the highest resolution shell. The original data set was reprocessed and therefore some of the parameters differ slightly from those given in Förster *et al.* (2006).

Space group	*C*2
Unit-cell parameters (Å, °)	a = 36.10, b = 38.92, c = 30.79, β = 110.61
Radiation source	ELETTRA, beamline XRD1
Wavelength (Å)	0.900
Resolution range (Å)	80.0–1.80 (1.83–1.80)
Matthews coefficient V_M (Å^3 Da^{-1})	2.31
Crystal mosaicity (°)	0.71
Total No. of reflections	12702
No. of unique observations	3677
Completeness (%)	98.9 (100)
Multiplicity	3.5 (3.1)
Average $I/\sigma(I)$†	14.9 (2.2)
R_{merge}‡ (%)	7.4 (23.6)
Molecules per ASU	1
Final R/R_{free}§ (%)	15.4/19.5
RNA atoms	292
Water O-atom loci	75
R.m.s.d. bond lengths (Å)	0.014
R.m.s.d. angles (°)	1.81

† Reflection intensity. ‡ $R_{merge} = \sum_{hkl}\sum_i |I_i(hkl) - \langle I(hkl)\rangle|/\sum_{hkl}\sum_i I_i(hkl)$, where $I_i(hkl)$ and $\langle I(hkl)\rangle$ are the observed individual and mean intensities of a reflection with indices *hkl*, respectively, $\sum_i$ is the sum over the individual measurements of a reflection with indices *hkl* and $\sum_{hkl}$ is the sum over all reflections. § R_{free} is based on 5% of the data selected with *REFMAC*5 (Murshudov *et al.*, 1997).

1976), we decided to generate a tRNA^{Ser} acceptor-stem microhelix model from a native tRNA structure. We chose the yeast tRNA^{Phe} as basis for our model. The final molecule used for molecular replacement, a seven-base-pair acceptor-stem microhelix, was generated from the coordinates of the re-investigated tRNA^{Phe} structure solved to 1.93 Å resolution (Shi & Moore, 2000; PDB code 1ehz). The base sequence in the model was converted to the correct sequence of the tRNA^{Ser} microhelix by exchanging the bases using the program *Coot* (Emsley & Cowtan, 2004). Using this method, nine bases were exchanged in the 7-mer helix at positions 2, 3, 6 and 7 in the 5′-strand and at positions 66, 67, 69, 70 and 71 in the 3′-pyriminine strand. The unequal number of exchanges is a consequence of the presence of a GU base pair in the initial tRNA^{Phe} microhelix. A total of 82 atoms have new locations in the generated tRNA^{Ser} microhelix model compared with the tRNA^{Phe} microhelix. Apart from roughly checking the geometry and the distances of the new constructed base pairing, the model was not further optimized and was used directly for molecular-replacement calculations.

The constructed tRNA^{Phe} microhelix without changing the sequence to that of the tRNA^{Ser} microhelix was initially tested as a model and gave no satisfying solution in molecular replacement. However, correction of the sequence to that of the tRNA^{Ser} microhelix resulted in successful molecular-replacement calculations. The initial R and R_{free} values after molecular replacement were 43.2% and 38.3%, respectively, using data in the resolution range 60–2.0 Å. The solution was clearly confirmed by the highest peak in the rotation function; the next highest peaks in the rotation function gave no solution in the translation search. Initial cycles of restrained refinement using the *CCP*4 program *REFMAC*5 (Murshudov *et al.*, 1997), applying standard angle geometries and bond lengths for sugars, backbone phosphates and nucleobases, resulted in R and R_{free} values of 24.6% and 29.0%, respectively. The program *Coot* was used for model building and refinement. Solvent molecules were introduced using the programs *Coot* and *ARP* (Lamzin & Wilson, 1993). Using all reflections up to the highest resolution shell (1.8 Å), R and R_{free} values of 15.4% and 19.5%, respectively, were obtained. The correctness of the final model was also confirmed by the low R_{free} value.

The helical parameters of the tRNA^{Ser} microhelix, as well as those of the selected reference molecules the tRNA^{Ala} microhelix (Müller *et al.*, 1999), the 5S RNA E-helix (Perbandt *et al.*, 2001) and the generated tRNA^{Phe} microhelix from native tRNA^{Phe} (Shi & Moore, 2000), were calculated with the program *X3DNA* (Lu & Olson, 2003) using the deposited coordinates of the structures.

3. Results

3.1. Overall crystal and RNA structure parameters

The tRNA^{Ser} acceptor-stem microhelix with sequence r(GGAGAGA)·r(UCUCUCC) from *Escherichia coli* was chemically synthesized, purified and crystallized as described previously (Förster *et al.*, 2006) and the structure was examined by X-ray crystallography. Crystallographic and X-ray diffraction parameters are summarized in Table 1.

The helix crystallizes in space group *C*2 with one molecule per asymmetric unit. The final R factor is 15.4% for 3494 reflections in the resolution range 17.5–1.8 Å, with a corresponding R_{free} of 19.5%. The root-mean-square (r.m.s.)

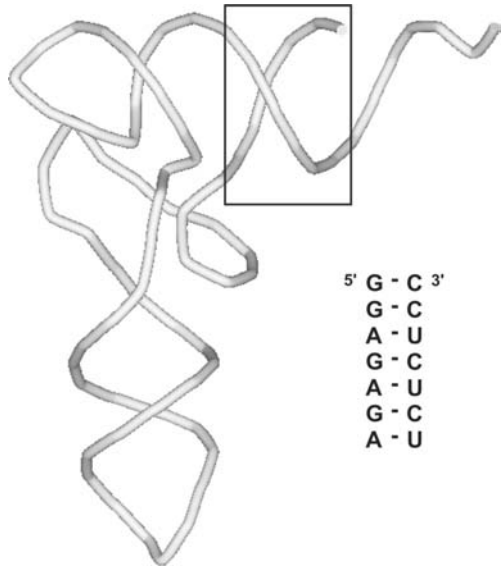

Figure 1
Representation of the tRNA-backbone conformation, highlighting the location of the acceptor-stem microhelix that provides important identity elements. The diagram is based on the tRNA^{Phe} crystal structure (PDB code 1ehz; Shi & Moore, 2000) and the sequence of the tRNA^{Ser} acceptor-stem microhelix structure reported here is given.

deviations for bond lengths and angles are 0.014 Å and 1.81°, respectively.

The crystal lattice consists of endless rows of RNA duplexes. The helices are related by a crystallographic twofold symmetry perpendicular to the helix axis. Two helices stack onto each other 'head-to-head'. We observe hydrophobic interactions of the 5′-guanosine in helix 1 with the 5′-guanosine in helix 2 (the sequence of the tRNA^{Ser} microhelix is shown in Fig. 1). This arrangement might be favoured energetically by interaction of the 5′ all-purine strands; the second strand of the helix consists of only pyrimidine bases. This leads to a continuing endless helix in the crystal lattice, which can be seen in Figs. 2(*a*) and 2(*b*). Fig. 2(*c*) demonstrates the stacking of the two first guanosines (5′-G1–G2) in helix 1 onto the top of the first two guanosines (5′-G1′–G2′) in helix 2. Packing between the other ends of the helix is a regular stacking interaction between 3′-A7–C66-5′ of the first helix with the 3′-A7–C66-5′ base pair of the second helix (the stacking of this part of the helix is not shown).

The asymmetric unit includes 292 RNA atoms of the single RNA duplex in conjunction with a hydration shell of 75 well defined water loci, of which three pairs of water positions are partially occupied. Although the tRNA^{Ser} microhelix was crystallized in the presence of magnesium ions, no such cations could be detected in the electron-density map. On detailed analysis of the solvent surrounding the RNA, no hexacoordinated ions could be detected.

3.2. Helical parameters

The helical parameters of the tRNA^{Ser} duplex are summarized and compared with those of other selected RNA crystal structures in Table 2. This comparison includes the tRNA^{Ala} acceptor-stem microhelix (Müller *et al.*, 1999), the 5S RNA E-helix (Perbandt *et al.*, 2001) and the native tRNA^{Phe} microhelix model generated from native tRNA^{Phe} (Shi & Moore, 2000). All RNA crystal structures presented here possess the canonical RNA conformation with minimal individual variances.

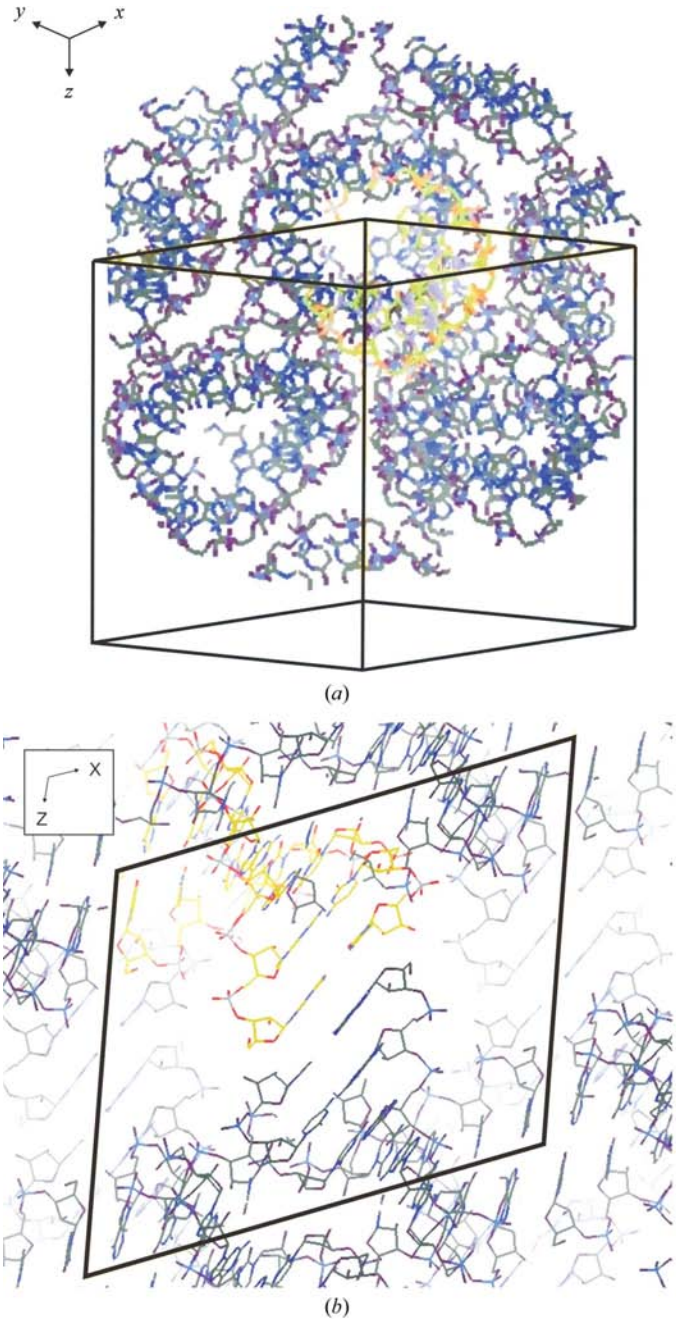

Figure 2
(*a*) Crystal packing of tRNA^{Ser} acceptor-stem helices; (*b*) and (*c*) detailed views of the stacking features. Lines indicate the unit cell of the monoclinic space group *C*2. Apparently 'endless' helices result from head-to-head and back-to-back contacts between the duplexes. While at the A7–U66 end one helix stacks 'regularly' against U66′–A7′ of another helix, the stacking at the other end is accompanied by a shift as illustrated in (*b*) and (*c*). This is presumably driven by a favourable G-stacking between the terminal guanosines.

Table 2
Selected average local base-pair parameters and global rise with standard deviations of the $tRNA^{Ser}$ acceptor-stem microhelix compared with the $tRNA^{Ala}$ microhelix (PDB code 434d; Müller *et al.*, 1999), the 5S RNA E-helix (PDB code 439d; Perbandt *et al.*, 2001) and the $tRNA^{Phe}$ microhelix generated from PDB code 1ehz (Shi & Moore, 2000).

All data in Tables 2, 3 and 4 were calculated from the deposited coordinates using *X3DNA* (Lu & Olson, 2003).

	Twist (°)	Rise (Å)	Slide (Å)	Roll (°)	*x* displacement (Å)	Propeller twist (°)
$tRNA^{Ser}$ microhelix	31.88 ± 3.78	2.71 ± 0.17	−1.62 ± 0.33	6.56 ± 2.25	−4.07 ± 1.36	−9.72 ± 4.55
$tRNA^{Ala}$ microhelix A	32.52 ± 3.50	2.57 ± 0.15	−1.59 ± 0.20	7.38 ± 1.58	−3.98 ± 0.80	−9.02 ± 3.19
$tRNA^{Ala}$ microhelix B	31.41 ± 2.78	2.68 ± 0.13	−1.56 ± 0.30	7.51 ± 3.52	−4.06 ± 1.21	−10.22 ± 4.81
5S RNA E-helix	31.48 ± 9.98	2.36 ± 0.10	−1.97 ± 0.41	7.97 ± 3.75	−5.53 ± 3.45	−11.31 ± 4.08
Generated $tRNA^{Phe}$ microhelix	32.54 ± 7.23	2.67 ± 0.24	−1.47 ± 0.24	8.42 ± 1.46	−3.97 ± 1.05	−12.17 ± 6.73

Table 3
Global helical twist and rise of the $tRNA^{Ser}$ acceptor-stem microhelix and local base-pair *x* displacement.

	Twist (°)	Rise (Å)	*x* displacement (Å)
G1–C72			
	32.71	2.55	−4.38
G2–C71			
	31.47	2.98	−2.97
A3–U70			
	27.56	2.74	−6.56
G4–C69			
	35.10	2.54	−3.33
A5–U68			
	32.92	2.82	−4.18
G6–C67			
	34.26	2.65	−3.01
A7–U66			

The $tRNA^{Ser}$ helix shows a conformation with all ribose residues having 3′-*endo*/2′-*exo* puckering and an average helical twist of 31.9° or approximately 11 residues per helical turn. The mean rise of 2.7 Å lies within the typical range as found in other RNAs. The mean slide of −1.62 Å and mean roll of 6.5° also lie within the expected range. The *x* displacement, which has an average value of −4.1 Å, and the average propeller twist of −9.7° also describe the conformation of an A-type duplex.

The local helical parameters of the $tRNA^{Ser}$ microhelix are given in Table 3. The twist and rise are in reasonable agreement with A-conformational RNA. The largest *x*-displacement value of −6.6 Å is observed for the step A3–U70 to G4–C69.

Interestingly, irregularities in the backbone torsion angles can be observed for part of the $tRNA^{Ser}$ 5′-strand and are highlighted in Table 4. For most of the backbone regions, the α backbone torsion angles are, as expected, in the g^+ conformation with values around −60° to −70°. All β backbone torsion angles are around ±180° and most γ angles are around 40–60° and show g^- conformation. However, the backbone of nucleotide G4 differs in overall conformation from standard A-type RNA. The α and γ backbone torsion angles of G4 adopt *trans* conformation values of around ±180° instead of the g^- conformation for the α angles and g^+ conformation for the γ angles found in A-RNA (Table 4).

The overall helix shows a bent conformation (Fig. 3*b*) that is characterized by the longest observed inter-phosphate distance in the molecule being in the 5′ all-purine strand between position G4 and A5, which is also the location of the unusual backbone torsion angles (Table 4). This corresponds to the shortest observed inter-phosphate distance in the molecule being in the opposing 3′ all-pyrimidine strand between nucleotides 71 and 70.

3.3. Hydration and ions

In the $tRNA^{Ser}$ acceptor-stem X-ray structure we detected a hydration shell consisting of 75 water loci per duplex, but we did not identify any ions. Fig. 3 presents a stereoview of the helix with all associated water loci (Fig. 3*a*) and highlights specially those that are located between the backbone phosphates (Fig. 3*b*) and within the base planes in the major groove (Fig. 3*c*) and minor groove (Fig. 3*d*). The schematic summary in Fig. 3(*e*) highlights two particular aspects. Firstly, the hydrogen-bonding potential of the major-groove and minor-groove edges of the individual bases can be observed to be fully utilized in most instances. Secondly, the distances between phosphate atoms correlate closely with their respective hydration pattern, a general feature that has been described for DNA conformations as 'the economy of water' (Saenger *et al.*, 1986). In the RNA structure presented here, three categories can be distinguished, two of which are in the pyrimidine strand. The 6.0–6.1 Å distance between the phosphate groups on either side of the C69 and U71 bases is bridged by a pair of partially occupied water loci that are about 2.2 Å apart. A second doubly bridged pattern consisting of a single and a connected pair of water molecules is observed for the 5.4–5.5 Å distance between the phosphate groups on either side of the U70 and C67 bases. Similar distances of 5.5–5.7 Å can be detected in the purine strand on either side of the G2, A3, A5 and G6 bases, which are also doubly bridged by two single water molecules. One of these waters is also within hydrogen-bonding distance of the N7 of the respective base, with the exception of G4, which exhibits an additional intervening water molecule. Either side of the G4 base, the P atoms are separated by the unusually extended distance of 6.9 Å, which is associated with a particularly large number of water loci within hydrogen-bonding distance of the A5 phosphate.

In the region that carries the identity elements responsible for seryl-tRNA interaction, a prominent hydrogen-bond network could be detected (shown in Fig. 4). This particular hydration pattern consists of two layers of coordinated water

molecules which cover the RNA phosphate-backbone region of nucleotides C67, U68, C69, U70 and C71.

4. Discussion

Here, we describe the high-resolution structure of an elongator tRNA^{Ser} acceptor-stem microhelix. This part of the tRNA carries specific identity elements that recognize the seryl-tRNA synthetase (Normanly *et al.*, 1986, 1992; Schimmel, 1987; Normanly & Abelson, 1989). Additionally, the long extra arm of tRNA^{Ser} contributes strongly to synthetase binding (Schatz *et al.*, 1991; Bilokapic *et al.*, 2006; Biou *et al.*, 1994; Cusack *et al.*, 1996), which is not the subject of the investigation presented here. tRNA^{Ser} microhelix isoacceptors can be specifically aminoacylated with serine (Sampson & Saks, 1993), which demonstrates that this part of the tRNA contains the unique determinants assuring the correct aminoacylation process.

Owing to redundancy in the genetic code, six serine codons and therefore six different seryl-tRNA isoacceptors exist (Sprinzl & Vassilenko, 2005), which all must carry the identity elements for serine aminoacylation. In addition, the selenocysteine-specific tRNA^{Sec} is also aminoacylated with serine prior to conversion to selenocysteinyl-tRNA^{Sec}; this is another tRNA that depends on seryl-tRNA synthetase interaction (Forchhammer *et al.*, 1991; Forchhammer & Böck, 1991).

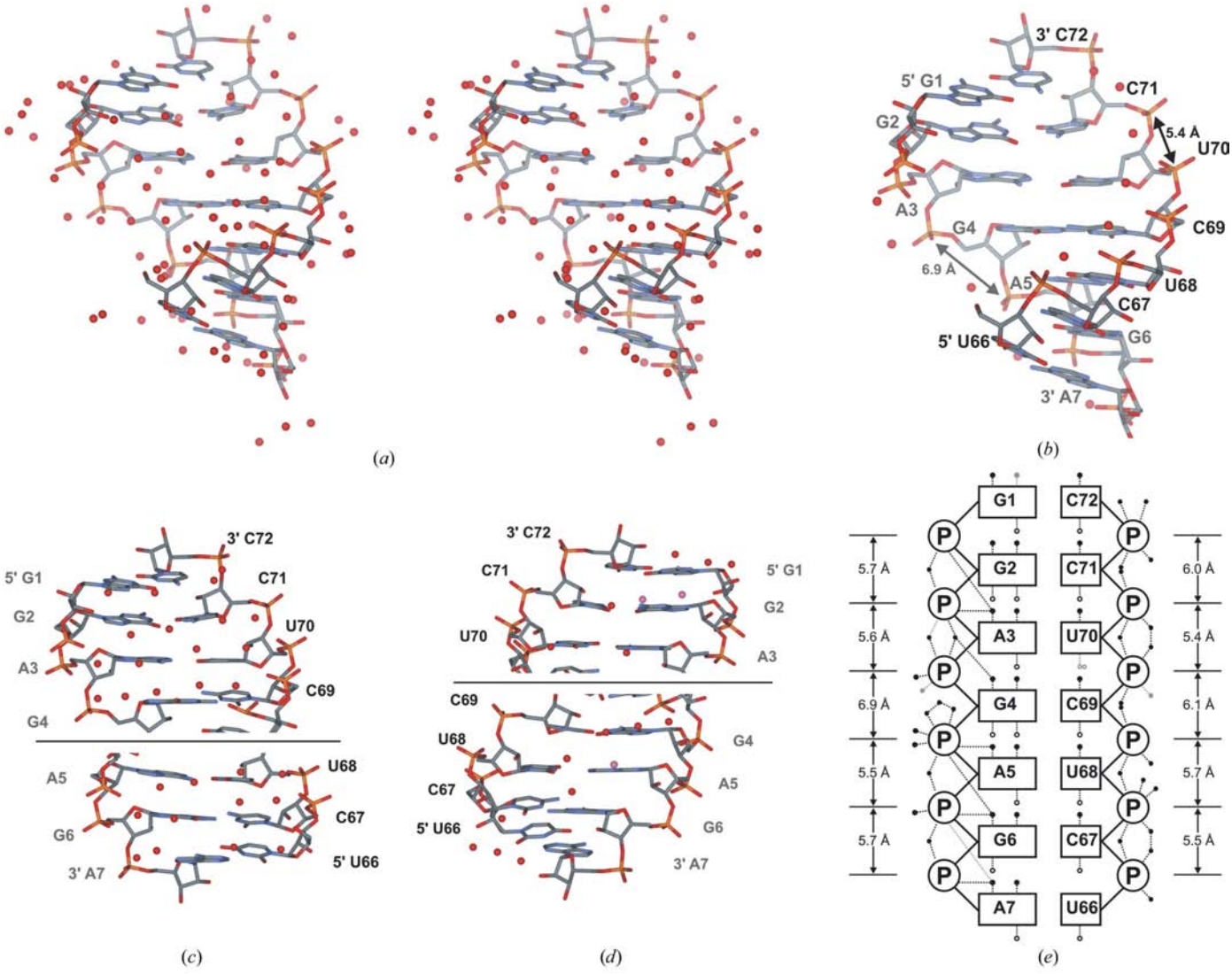

Figure 3
(*a*) Stereo representation of the tRNA^{Ser} acceptor-stem microhelix structure with the 75 associated water loci. (*b*) The same view as in (*a*) with sequentially labelled nucleotides, showing only selected water loci between neighbouring phosphate groups. The longest and shortest sequential interphosphate distances within the helix are highlighted; these are indicative of the particular kink within this microhelix. (*c*) and (*d*) Water loci located in the plane of the bases in the major and minor groove, respectively. For each groove, views of two differently rotated segments (separated by a horizontal line) are shown for clarity; symmetry-related water molecules are shown in pink. (*e*) Schematic summary of water loci within hydrogen-bonding distance of the bases and backbone phosphate atoms O1P and O2P (summarized as P). Bases are represented by sequentially labelled squares, with major-groove and minor-groove edge contacts being indicated by filled and open circles, respectively. Black and grey dotted lines indicate distances within and marginally above a 3.5 Å cutoff, respectively; double circles represent neighbouring partially occupied water loci. The pattern of phosphate hydration correlates closely with the indicated distances between neighbouring phosphate atoms.

Table 4
Local backbone parameters of the tRNA^{Ser} acceptor-stem microhelix.

The irregular conformations compared with canonical A-form RNAs are highlighted in bold and discussed in the text.

	α (°)	β (°)	γ (°)
Strand 1			
G1	—	—	49.8
G2	−67.4	180.0	56.1
A3	−71.4	−177.6	47.8
G4	**144.0**	−167.2	**−174.2**
A5	−67.2	−174.3	40.2
G6	−63.7	170.4	51.9
A7	−61.2	171.2	52.1
Strand 2			
C72	−65.6	174.5	50.2
C71	−59.7	159.9	55.0
U70	−74.5	−175.9	49.1
C69	−61.5	166.3	57.6
U68	−70.2	172.3	52.1
C67	−69.8	177.2	53.1
U66	—	—	44.7

We chose the two seryl-tRNA isoacceptors with the highest possible sequence similarity to the selenocysteine-specific tRNA^{Sec} for structural analysis in order to compare the specific identity elements for aminoacylation with serine (Förster *et al.*, 2006), but only that presented here produced crystals suitable for X-ray analysis.

There is particular interest in investigating tRNA identity elements with respect to aminoacylation. In class II tRNA synthetases, important determinants are located in the aminoacyl region of the corresponding tRNAs, which makes the aminoacyl stem a valuable tool for structural investigation. In particular, the structure of the identity elements in tRNA^{Ser} will help in understanding the specific interactions with the synthetase. On the one hand, these have to allow the aminoacylation of all of the different tRNA^{Ser} isoacceptors and also of tRNA^{Sec}, but on the other they also have to assure the specificity of the process in order to avoid mis-aminoacylation.

Valuable structural information concerning tRNA^{Ser}–seryl-tRNA synthetase interaction already exists. Apart from the long unique variable extra arm of the tRNA, which makes contact with the special α-helical extra domain of seryl-tRNA synthetase by RNA-backbone interactions, there are interactions between the aminoacyl stem 3′-strand and the loop 2 motif of seryl-tRNA synthetase (Cusack *et al.*, 1996). However, as detailed information concerning the local helical parameters of the tRNA^{Ser} acceptor stem is lacking and the role of solvent molecules within this region is unknown, we focused our investigations on examining the structure of a tRNA^{Ser} acceptor-stem microhelix to high resolution. Here, we report the analysis of specific structural elements of a tRNA^{Ser} microhelix with regard to helical parameters and the role of hydrating water molecules.

Overall, the tRNA^{Ser} microhelix exhibits the typical A-type RNA conformation. However, in two regions of the RNA helix we observed a minimal deviation from standard A-RNA geometry. This was located in the backbone region within the 5′-strand of the acceptor stem, with the 5′-phosphate of nucleotide G4 not showing the usual g^- conformation; instead, the α- and γ-backbone torsion angles adopt *trans* conformations of around $\pm180^\circ$. This corresponds to a kinked irregularity in the RNA backbone. The role of RNA-backbone irregularities has been widely discussed, for example in the case of the tRNA^{Ala} identity. The unique base pair G3–U70 is alone responsible for determining tRNA^{Ala} specificity (Hou & Schimmel, 1988). Several research groups favour the idea that the exocyclic amino group of G3 is the specific recognition element for the aminoacyl-tRNA synthetase (Musier-Forsyth *et al.*, 1991, 1995; Beuning, Gulotta *et al.*, 1997; Beuning, Yang *et al.*, 1997). On the other hand, biochemical studies hint at the possibility that it is not the G3–U70 base pair itself but rather an RNA phosphate-backbone irregularity induced by the GU base pair that might be the recognition element for the protein (McClain *et al.*, 1988, 1996; Gabriel *et al.*, 1996), highlighting the importance of RNA backbone-mediated interactions with the synthetase. The tRNA^{Ser}–seryl-tRNA synthetase structures (Biou *et al.*, 1994; Cusack *et al.*, 1996) and the archea-bacterial seryl-tRNA synthetase structure with superimposed tRNA^{Tyr} (Bilokapic *et al.*, 2006) show that the 3′-strand of the tRNA acceptor stem makes a direct interaction with the seryl-tRNA synthetase. This contrasts with the 5′-strand of tRNA^{Ser} acceptor stem, which is mainly exposed to the solvent.

We also investigated the special role of water molecules in the structure of the tRNA^{Ser} microhelix. We identified 75 distinct water loci per helix, the majority of which could be described by some basic classifications (Fig. 3). Fig. 4 shows the hydrogen-bonding network of water molecules associated with the phosphate groups of C67, U68, C69, U70 and C71. In this case, we observe two layers of coordinated water molecules that represent a hydration pattern in the region of the free uncomplexed tRNA^{Ser} acceptor stem that is known to be a contact site for the synthetase. In order to investigate the interaction between the tRNA^{Ser} microhelix and seryl-tRNA synthetase in detail, docking experiments between the tRNA^{Ser} acceptor-stem helix and tRNA^{Ser}-interacting proteins are in progress.

The specific hydration pattern of the tRNA^{Ser} microhelix is likely to play an important role in the determination of RNA–

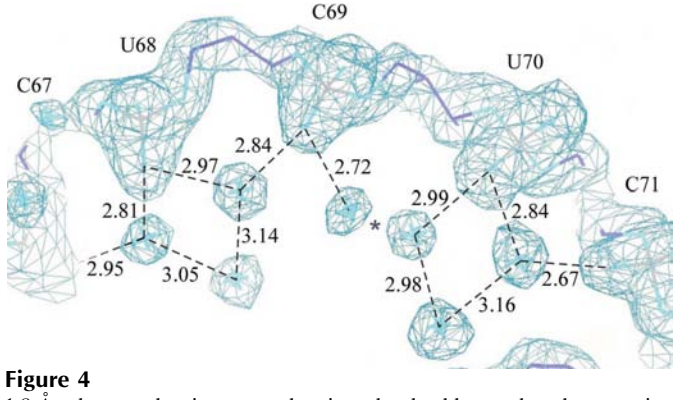

Figure 4
1.8 Å electron-density map showing the backbone-phosphate region between C67 and C71 of the 3′-strand of tRNA^{Ser} acceptor-stem helix and the coordinated water molecules. Hydrogen bonds are indicated by dashed lines and distances are given in angstroms. Near U70, there are two partially occupied alternative water molecule loci either side of the asterisk.

protein interactions. A special role may be associated with the two layers of coordinated water molecules along the $tRNA^{Ser}$ acceptor-stem backbone at the synthetase-recognition site. As the first contact to the protein is likely to be mediated by water molecules located in this region of the $tRNA^{Ser}$ microhelix, these may even direct the specific molecular recognition.

In summary, the crystal structure of the $tRNA^{Ser}$ microhelix presented here shows an unusual backbone conformation in the regions that are important for the interaction of the $tRNA^{Ser}$ with the seryl-tRNA synthetase. In addition, a characteristic hydration pattern is detected at this binding site. These features may represent previously unobserved structural determinants for specific molecular recognition between $tRNA^{Ser}$ and seryl-tRNA synthetase and may therefore contribute to further detailed understanding of the mechanisms that govern $tRNA^{Ser}$ aminoacylation, synthetase and elongation-factor recognition. We performed superposition experiments between the $tRNA^{Ser}$ microhelix presented here and the $tRNA^{Ser}$–seryl-$tRNA^{Ser}$ synthetase complex described by Biou *et al.* (1994), with which we could visualize the interface between the $tRNA^{Ser}$ microhelix and the synthetase as described in Förster *et al.* (2007). To this end, further crystallographic and docking experiments are in progress, with a focus on the water molecules surrounding the $tRNA^{Ser}$ microhelix.

This work was funded within the RiNA network for RNA technologies by the Federal Ministry of Education and Research, the City of Berlin and the European Regional Development Fund. We gratefully acknowledge the ELETTRA synchrotron, Trieste for providing beamtime and the European Union for reimbursement under EU contract RII3-CT-2004-506008 (IA-SFS), Fonds der Chemischen Industrie (Verband der Chemischen Industrie eV) and National Foundation for Cancer Research, USA for additional support and Jan Barciszewski for helpful discussions.

References

Beuning, P. J., Gulotta, M. & Musier-Forsyth, K. (1997). *J. Am. Chem. Soc.* **119**, 8397–8402.
Beuning, P. J., Yang, F., Schimmel, P. & Musier-Forsyth, K. (1997). *Proc. Natl Acad. Sci. USA*, **94**, 10150–10154.
Bilokapic, S., Korencic, D., Söll, D. & Weygand-Durasevic, I. (2004). *Eur. J. Biochem.* **271**, 694–702.
Bilokapic, S., Maier, T., Ahel, D., Gruic Sovulj, I., Söll, D., Weygand-Durasevic, I. & Ban, N. (2006). *EMBO J.* **25**, 2498–2509.
Biou, V., Yaremchuk, A., Tukalo, M. & Cusack, S. (1994). *Science*, **263**, 1404–1410.
Böck, A., Forchhammer, K., Heider, J., Leinfelder, W., Sawers, G., Veprek, B. & Zioni, F. (1991). *Mol. Microbiol.* **3**, 515–520.
Collaborative Computational Project, Number 4 (1994). *Acta Cryst.* D**50**, 760–763.
Cusack, S., Yaremchuk, A. & Tukalo, M. (1996). *EMBO J.* **15**, 2834–2842.
Emsley, P. & Cowtan, K. (2004). *Acta Cryst.* D**60**, 2126–2132.
Eriani, G., Delarue, M., Poch, O., Gangloff, J. & Moras, D. (1990). *Nature (London)*, **347**, 203–206.
Förster, C., Brauer, A. B. E., Fürste, J. P., Betzel, C., Weber, M., Cordes, F. & Erdmann, V. A. (2007). *Biochem. Biophys. Res. Commun.* **362**, 415–418.
Förster, C., Krauss, N., Brauer, A. B. E., Szkaradkiewicz, K., Brode, S., Hennig, K., Fürste, J. P., Perbandt, M., Betzel, C. & Erdmann, V. A. (2006). *Acta Cryst.* F**62**, 559–561.
Forchhammer, K. & Böck, A. (1991). *J. Biol. Chem.* **266**, 6324–6328.
Forchhammer, K., Boesmiller, K. & Böck, A. (1991). *Biochimie*, **73**, 1481–1486.
Gabriel, K., Schneider, J. & McClain, W. H. (1996). *Science*, **12**, 195–197.
Giegé, R., Sissler, M. & Florentz, C. (1998). *Nuclec Acids Res.* **26**, 5017–5035.
Hou, Y. M. & Schimmel, P. (1988). *Nature (London)*, **333**, 140–145.
Kim, S.-H., Suddath, F. L., Quigley, G. J., McPherson, A., Sussman, J. L., Wang, A. H.-J., Seeman, N. C. & Rich, A. (1974). *Science*, **185**, 435–440.
Korencic, D., Polycarpo, C., Weygand-Durasevic, I. & Söll, D. (2004). *J. Biol. Chem.* **279**, 48780–48786.
Lamzin, V. S. & Wilson, K. S. (1993). *Acta Cryst.* D**49**, 129–147.
Leinfelder, W., Zehelein, E., Mandrand-Berthelot, M. A. & Böck, A. (1988). *Nature (London)*, **331**, 723–725.
Lu, X.-J. & Olson, E. K. (2003). *Nucleic Acids Res.* **17**, 5108–5121.
McClain, W. H., Chen, Y.-M., Foss, K. & Schneider, J. (1988). *Science*, **242**, 1681–1684.
McClain, W. H., Gabriel, K. & Schneider, J. (1996). *RNA*, **2**, 105–109.
Müller, U., Schübel, H., Sprinzl, M. & Heinemann, U. (1999). *RNA*, **5**, 670–677.
Murshudov, G. N., Vagin, A. A. & Dodson, E. J. (1997). *Acta Cryst.* D**53**, 240–255.
Musier-Forsyth, K., Shi, J. P., Henderson, B., Bald, R., Fürste, J. P., Erdmann, V. A. & Schimmel, P. (1995). *J. Am. Chem. Soc.* **117**, 7253–7254.
Musier-Forsyth, K., Usmann, N., Scaringe, S., Doudna, J., Green, R. & Schimmel, P. (1991). *Science*, **253**, 784–786.
Navaza, J. (1994). *Acta Cryst.* A**50**, 157–163.
Normanly, J. & Abelson, J. (1989). *Annu. Rev. Biochem.* **58**, 1029–1049.
Normanly, J., Ogden, R. C., Horvath, S. J. & Abelson, J. (1986). *Nature (London)*, **321**, 213–219.
Normanly, J., Ollick, T. & Abelson, J. (1992). *Proc. Natl. Acad. Sci. USA*, **89**, 5680–5684.
Otwinowski, Z. & Minor, W. (1997). *Methods Enzymol.* **276**, 307–326.
Perbandt, M., Vallazza, M., Lippmann, C., Betzel, C. & Erdmann, V. A. (2001). *Acta Cryst.* D**57**, 219–224.
Quigley, G. J. & Rich, A. (1976). *Science*, **194**, 796–806.
Saenger, W., Hunter, W. N. & Kennard, O. (1986). *Nature (London)*, **324**, 385–388.
Sampson, J. R. & Saks, M. E. (1993). *Nucleic Acids Res.* **21**, 4467–4475.
Schatz, D., Lebermann, R. & Eckstein, F. (1991). *Proc. Natl Acad. Sci. USA*, **88**, 6132–6136.
Schimmel, P. (1987). *Annu. Rev. Biochem.* **56**, 125–158.
Shi, H. & Moore, P. B. (2000). *RNA*, **6**, 1091–1105.
Sprinzl, M. & Vassilenko, K. S. (2005). *Nucleic Acids Res.* **33**, D139–D140.
Sunharadas, G., Katze, J. R., Söll, D., Konigsberg, W. & Lengyel, P. (1968). *Proc. Natl Acad. Sci. USA*, **61**, 693–700.